Digital twin of ball bearing for predicting EHD lubrication regimes by DEM

S. OMAR FARAH[a,b], M. GUESSASMA[a], E. BELLENGER[a]

a. Campus Universitaire - LTI-EA3899, 48 rue d'Ostende, 02315 Saint-Quentin, France
samatar.omar.farah@etud.u-picardie.fr, mohamed.guessasma@u-picardie.fr,
emmanuel.bellenger@u-picardie.fr
b. Université de Djibouti, avenue Djanaleh BP 1904, Djibouti, Djibouti

Abstract

This work deals with the elastohydrodynamic (EHD) lubrication in ball bearing by means of a digital twin. Based on an original description involving discrete element method (DEM), the digital twin integrates all components of ball bearings and allows to achieve a realistic behavior under mechanical loading and kinematic conditions. In order to check the standard indicators recommended by most ball bearing manufactures, a stiffness model for elliptical Hertzian contact and an improved EHD formulation for lubricated contact are implemented in the numerical tool. In addition, we have introduced in the discrete modeling an electrical capacitance model correlated to the fluid film thickness and the contact pressure. The numerical predictions of lubricant film capacitance provided by digital twin are in good accordance qualitatively, or even quantitatively, with experimental data available in the literature. The coupling of the discrete method with the electrical approach, it gives the opportunity to provide efficient solutions in terms of lubrication regime in relation to the lubricant properties to optimize the bearings lifetime.

Mots clefs : Ball bearings, DEM, EHD lubrication, tribology, fluid film, electrical capacitance

1 Introduction

Industrial machines need a good lubrication regime with an appropriate lubricant to avoid wear mechanisms that could occur at the contact interface between two surfaces. In rotating machines several components such as ball bearings, cams and gears operate under EHD lubrication regimes with nonconformal contacts. The nonconformity of the surfaces in contact means that the contact areas are subjected to a high contact pressure that can be in the range of several gigapascals. With a view to be able to assess if the machine elements are working with safety conditions or they are close to reach boundary lubrication and ultimate failure, the fluid film thickness is consequently of a prime importance. Such mechanical components are often designed for the lubricant film to be thick enough, more than $1\ \mu m$, to avoid contact between the mating surfaces ensuring the expected bearing lifetime. For that purpose several experimental methods are dedicated to measure the lubricant film thickness. The most widely used one is based on optical interferometry [1, 2]. In the area of ball bearing diagnosis, the electrical

techniques have been used to measure the load distribution by capacitance sensors [3] as well as to highlight the angular speed effect on the lubrication regime by means of the electrical resistance [4]. More recently, Jablonka *et al.* [5] proposed a quantitative evaluation of lubricant film thickness in a radially loaded deep-groove ball bearing using electrical capacitance measurements. The authors used an in-situ monitoring tool in order to identify the lubrication conditions as function to the operating parameters and lubricant properties.

Recently the DEM has been used successfully for simulating the dynamic behavior of bearings with tribology enrichments [6] as weel as for modeling lubrication regimes by means of an EHD model [4]. To achieve this proposal, the digital twin of ball bearings implements a major part of the functionalities according to the state of the art, such as the slice model, the mutual influences of neighboring elements with clearance, elliptical Hertzian contact model, lubricant film estimation, damping forces, centrifugal forces, etc. In the present study, the ball bearing is simulated with the assumption of EHD lubrication conditions. The coupling between the mechanical pressure and the dielectric behavior of the lubricant film thickness is carried out by means of the electrical capacitance. According to the model of two parallel-plate capacitor separated by a dielectric material, the capacitance of the lubricant film thickness is extracted numerically. The numerical predictions of fluid film capacitance for the two simulated lubricants provide a promising result in comparison to the experimental data available in the bibliography [5].

2 Digital twin of radial ball bearing

A three-dimensional digital twin of ball bearing (Fig. 1-a) is developed by means of MULTICOR3D software using DEM [7]. The radial ball bearing of 6208 series (SKF 6208 TN9/DBGA) has been considered in the present study (Fig. 1-b). The dimensions and geometrical conformity of the 6208 radial ball bearing are provided in table 1. The number of rolling elements which are likely to be in contact with the inner or outer raceways is $Z = 9$. Furthermore, nine additional smaller balls of radius R_z in contact with two toruses are considered to reproduce the cage effects (Fig. 2). Even if the cage is different in shape in comparison to the standard form, the design does not at all affect the contact forces between rolling elements and cage.

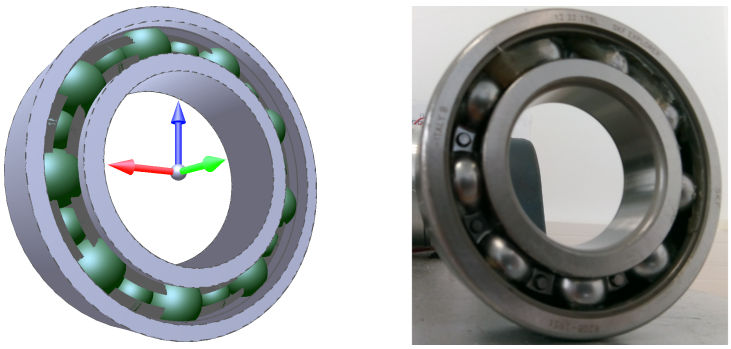

(a) (b)

Figure 1: (a) Digital twin of radial ball bearing of 6208 series - (b) SKF radial ball bearing of 6208 series

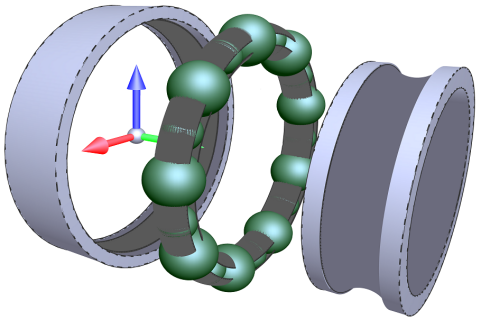

Figure 2: Exploded view of digital twin of radial ball bearing of 6208 series

We note that this description of the cage mainly has two roles. The first is that it ensures a conform internal radial load distribution, while the second is that it allows intermittent rolling elements/cage contacts to be taken into account when the ball bearing operates. However, details should be supplied about the cage in the sense that the only other possible interactions involving the cage balls may be occur with rolling elements. By considering all bearing components, the proposed modeling gives the opportunity to develop a digital twin without any restriction.

Component	Rolling element	Inner ring	Outer ring	Raceways	Cage
Radius	R_b	R_i	R_e	$R_c^i = R_c^o$	R_z
Dimension (mm)	6.3	24.0	36.6	6.552	4.19

Table 1: Geometric characteristics of 6208 radial ball bearing

3 Mechanical modeling of contact forces

The contact stiffness model that we used is based on a smoothed formulation of DEM initially proposed by Cundall and Strack [8]. The contact interactions are obtained by means of Kelvin-Voigt Spring-Dashpot Model and a Coulomb's law if sliding occurs at the contact (Fig. 3). The main assumption made with DEM is that the particles in contact are assumed perfectly rigid and therefore, there is no elastic deformation of all bearing components. The elasticity is only considered at the contact between, rolling element/raceways (inner or outer), cage ball/toruses and rolling element/cage ball (Fig. 2).

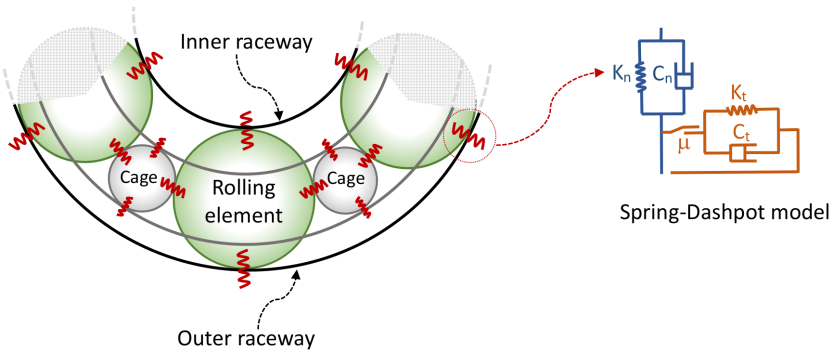

Figure 3: Contact stiffness model

3.1 Hertzian contact stiffness model

The contact forces $F_{n,t}$ in normal and tangential directions according to the local frame at the contact plane, are described with an explicit mechanical model depending on elastic force displacement law, Coulomb friction and viscous damping coefficients (1).

$$\begin{cases} F_{n,t} = K_{n,t}\,\delta_{n,t} + C_{n,t}\,v_{n,t} \\ \text{with} \\ F_t = -min\left(F_t,\,\mu F_n\right) \times sgn\left(v_t\right) \end{cases} \tag{1}$$

with $K_{n,t}$ the normal and tangential stiffnesses, $C_{n,t}$ the normal and tangential viscous damping coefficients, $\delta_{n,t}$ the normal and tangential relative displacements, $v_{n,t}$ the normal and tangential relative speeds according to the local frame and μ the Coulomb friction coefficient in the case of a sliding contact. The normal viscous damping coefficient C_n to ensure a mechanical steady state is function of two damping types, namely hysteretic and EHD, related to the contact shape, roughness, fluid viscosity, temperature, entrainment speed, etc. The tangential viscous damping coefficient C_t is more difficult to evaluate. The ratio $\frac{C_t}{C_n}$ is usually considered to range in the interval $[0,\ 1]$. The normal contact stiffness K_n is related to mechanical characteristics and curvatures of the surfaces in contact according to non-linear model ; $F_n \propto \delta_n^{3/2}$. For a given rolling element in contact with inner-raceway (or outer-raceway), with the assumption of an elliptical Hertzian contact, the normal stiffness is written as function of the curvature sum radius and the approximate elliptic integrals as introduced by Hamrock [9]:

$$\begin{cases} K_n = \frac{2\pi\kappa G}{1-\nu}\sqrt{\frac{2\overline{\mathcal{E}}R_{curve}}{9\overline{\mathcal{F}}^{\,3}}}\;\delta_n^{1/2} \\ R_{curve} = \frac{R_x R_y}{R_x + R_y} \\ R_x = \frac{R_{1x}R_{2x}}{R_{2x} \pm R_{1x}},\ R_y = \frac{R_{1y}R_{2y}}{R_{2y} - R_{1y}} \end{cases} \tag{2}$$

where R_{curve} is the curvature sum radius, R_x the effective radius in x direction, R_y the effective radius in y direction, κ the ellipticity parameter $\left(\kappa = \alpha^{\frac{2}{\pi}},\ \alpha = \frac{R_y}{R_x}\right)$, $\overline{\mathcal{F}}$ the approximate elliptic integral of first kind $\left(\overline{\mathcal{F}} = 1 + q\ ln\ \alpha,\ q = \frac{\pi}{2} - 1\right)$ and $\overline{\mathcal{E}}$ the approximate elliptic integral of second kind $\left(\overline{\mathcal{E}} = 1 + \frac{q}{\alpha}\right)$ (Fig. 4). The equivalent radius R_x is calculated by taking into account the cases of convex contact (rolling element/inner-raceway) and concave contact (rolling element/outer-raceway), as given in equation (2). For the sake of clarity, we note that $R_b = R_{1x} = R_{1y}$, $R_{2x} = R_i$ and $R_{2y} = R_r$. $G = \frac{E}{2(1+\nu)}$ is the shear modulus of steel in the case of identical materials in contact, E the Young's modulus ($E = 210$ GPa) and ν the Poisson's ratio ($\nu = 0.3$).

When interactions between rolling element and cage ball occur the contact is assumed to be without friction and the damping coefficient is considered critical. The normal stiffness (3) is only taken into account, and therefore the following equation is considered [10]:

$$K_n = \frac{4E_{eq}\sqrt{R_{eq}}}{3\left(1-\nu\right)}\;\delta_n^{1/2} \tag{3}$$

with E_{eq} the equivalent Young's modulus $\left(\frac{1}{E_{eq}} = \frac{1-\nu^2}{E} + \frac{1-\nu_c^2}{E_c}\right)$, E_c the Young's modulus ($E_c = 3.3$ GPa) and ν_c the Poisson's ratio ($\nu_c = 0.41$) of cage balls made with polyamide 66 (PA66), $R_{eq} =$

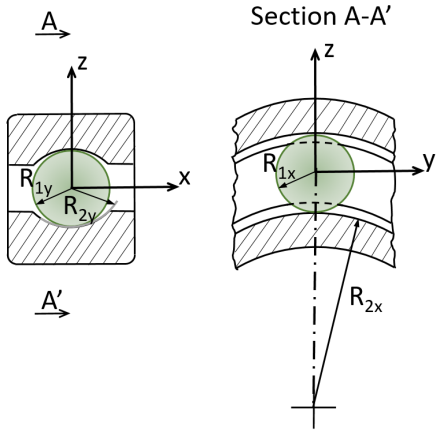

Figure 4: Curvatures in contact in two orthogonal cross sections of a ball bearing: (a) $x-z$ plane - (b) $y-z$ plane

$\frac{r_i r_j}{r_i+r_j}$ the equivalent radius of rolling element and cage ball in contact of radius r_i and r_j, respectively. To achieve a steady regime of the ball bearing under operating conditions, viscous damping and local friction are added as dissipative forces to the mechanical model (1). When a contact occurs between rolling element and raceways (inner or outer) two kinds of normal viscous damping could be involved: hysteritic and(or) fluid. The viscous effect due to the hysteretic damping, which is related to the plastic strain of surface roughness (4), is expressed by the coefficient C_{hyst} in the normal direction $\vec{n}$.

$$C_{hyst} = \frac{3\alpha_e K_n \delta_n}{2} \tag{4}$$

where α_e denotes the restitution coefficient of steel [11]. A value of $0.08\ s.m^{-1}$ is considered to compute the hysteritic damping C_{hyst}.

Regarding the viscous damping due to the fluid film, Walford and Stone [12] established a damping coefficient C_{fluid} related to the lubrication film in the normal direction of contact (5). Since the bearing contains non-conformal contacts endowed with EHD lubrication regime, the lubricant film must be thick enough to avoid contact between the mating surfaces.

$$C_{fluid} = \frac{3\pi\eta a}{\sqrt{2}} \left(\frac{R_b}{h_{min}}\right)^{3/2} \tag{5}$$

where η is the dynamic viscosity of the fluid at operating temperature and atmospheric pressure [13], a the semi-major axis of the Hertz's elliptical contact [14], h_{min} the minimum lubricant film thickness of the ball-inner-raceway (or -outer-raceway) contact.

The DEM modeling is by solving Newton's second law for each rolling element taking into account dynamical effects, such as centrifugal forces and gyroscopic effects, when the bearing is functioning. The mechanical resolution requires an explicit time integration based on the velocity-Verlet scheme.

3.2 EHD lubrication model

In the field of EHD lubrication, oil (or grease) rheology influences the fluid film thickness under operating conditions [15]. Given that the viscosity of lubricant increases with respect to pressure, this means that the lubricant exhibits piezo-viscous behavior. Furthermore, temperature also plays a role in lubricant viscosity changes with the consequence of a diminishing its viscosity. Starting from these assumptions with a piezo effect of the lubricant, we have implemented in the digital twin an EHD model with piezo-viscous-elastic regime to predict the minimum fluid film thickness h_{min} (6). As initially proposed by Hamrock and Anderson [9], the general form of the EHD model is function of parameters related to the speed, load and material properties. Relativley Recently, Masjedi and Khonsari [16] improved the EHD model by introducing the ellepticity effect. Since changing bearing conformity affects the contact ellipticity, we have implemented in the digital twin the new EHD formulation in which the parameters of the model are function of the ellepticity. In the case of smooth point-contact EHD the expression of the minimum fluid film thickness is as follows:

$$\frac{h_{min}}{R_x} = 1.637\,\overline{U}_r^{\,0{,}711\kappa^{-0{,}023}}\,\overline{E}^{\,0.65\kappa^{-0.045}}\,\overline{W}^{\,-0.09\kappa^{-0.15}}\left(1-0.974e^{-0.676\kappa}\right) \tag{6}$$

where $\overline{E}$, $\overline{U}_r$, $\overline{W}$ are three dimensionless parameters: $\overline{E} = \xi E'$, with ξ the pressure-viscosity coefficient of the lubricant at operating temperature and atmospheric pressure, $E' = \frac{E}{1-\nu^2}$ the effective elastic modulus of steel ; $\overline{U}_r = \frac{\eta U_r}{E' R_x}$, with U_r the entrainment speed ; $\overline{W} = \frac{Q_\psi}{E' R_x^2}$, with Q_ψ the ball-inner-raceway (or -outer-raceway) normal load at an azimuth angle ψ (Fig. 5-a).

It is commonly agreed that the identification of the lubrication regime in which a system is running in is by the use of the dimensionless fluid parameter Λ_f such defined by (7). Λ_f is the ratio of the minimum fluid film thickness to the surface roughness [17]:

$$\Lambda_f = \frac{h_{min}(Q_\psi, \omega)}{\sqrt{\sigma_1^2 + \sigma_2^2}} \tag{7}$$

where σ_1 and σ_2 denote the standard mean roughnesses of the measured surfaces for the inner-raceway (or outer-raceway) and rolling elements, respectively. However it is admitted that only the raceways roughness is considered and the rolling element roughness could be then neglected ($\sigma_2 << \sigma_1$). In addition, the schematic representation of the Stribeck curve (Fig. 5-b) for non-conformal contact shows the dependence of the friction coefficient μ on the dimensionless fluid parameter Λ_f. The friction coefficient μ is therefore depending on the regime of lubrication [18]. In addition, the Stribeck curve (Fig. 5-b) defines mainly three lubrication regimes (boundary, mixed-film or fully-fluid film) in relation to fluid parameter Λ_f.

3.3 Electrical capacitance model for lubricated Hertzian contact

In the context of the identification of lubrication film by means of electrical measurements, the fluid film thickness can be easily extracted from the capacitance of the contact [19]. According to the parallel-plate formula the lubricant film thickness is inversely proportional to the capacitance (8).

$$C_{Hertz} = \varepsilon_0 \varepsilon_r \frac{A_{Hertz}}{h_c} \tag{8}$$

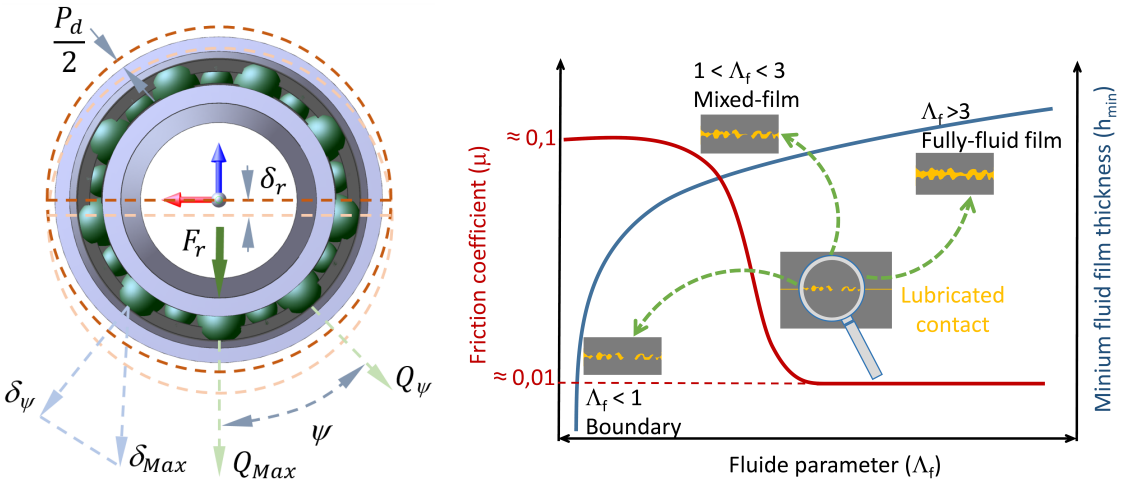

(a) (b)

Figure 5: (a) Radial shift δ_r due to the imposed radial load F_r and diametral clearance P_d - (b) Schematic representation of Stribeck curve: friction coefficient and fluid film thickness as function of fluid parameter

with C_{Hertz} the Hertzian contact capacitance between two parallel conducting plates of area A_{Hertz} separated by a dielectric material where ε_r is the dielectric constant of the fluid and h_c its central thickness. ε_0 is the vacuum permitivity $\left(\varepsilon_0 = 8.854\, pF.m^{-1}\right)$. The theoretical form of the contact area between the rolling element and raceway for a perfect elliptical Hertzian contact is $A_{Hertz} = \pi ab$, with a and b the major and minor semi-axes of the ellipse, respectively. In the case of smooth surface [16] the central film fluid thickness h_c integrating the ellepticity effect is as follows (9):

$$\frac{h_c}{R_x} = 3.672\, \overline{U}_r^{\,0,663\kappa^{-0,025}}\, \overline{E}^{\,0.502\kappa^{-0.064}}\, \overline{W}^{\,-0.045\kappa^{-0.18}} \left(1 - 0.573e^{-0.74\kappa}\right) \tag{9}$$

From experimental stand point, the qualitative conversion of the measured capacitance to lubricant film thickness involves first the estimation of the capacitance related to the nearly area outside the Hertzian contact and some background capacitance. The two latter are then subtracted from all measurement data. The remaining value corresponds to the contact capacitance due to the fluid flim thickness [20]. From a numerical point of view, the contact capacitance is easily computed from expression (8) after predicting central fluid film thickness by (9).

The dielectric constant ε_r of the lubricants varies with Hertz contact pressure. For nonpolar lubricants ε_r can be calculated from Clausius-Mossotti model [21]:

$$\frac{\varepsilon_r - 1}{\varepsilon_r + 2} = \frac{N_A \beta \rho}{3M} \tag{10}$$

where N_A is the Avogadro number, β the molecular polarizability, M the molecular weight and ρ the density. The factor $\frac{N_A\beta}{3M}$ can be deduced by considering permittivity and density at atmospheric pressure. According to the formula established by Dowson and Higginson [22], the variation of the lubricant density as function of the contact pressure is given by following equation (11):

$$\rho = \rho_0 \frac{0.59 \cdot 10^9 + 1.34 \cdot P_{Hertz}}{0.59 \cdot 10^9 + P_{Hertz}} \tag{11}$$

with ρ_0 the ambient-pressure density and P_{Hertz} the Hertz contact pressure. In Figure 6-a are plotted the dielectric constant evolution of synthetic oil film (Tab. 2) with respect to Hertz contact pressure at inner and outer raceways. This can be easily understood by the fact that the higher a pressure is, the greater is the dielectric constant of the lubricant film. As depicted by the curves in Figure 6-b, the maximum Hertz contact pressure at the inner raceway is greater than reached at the outer raceway due to the difference of the ellepticity of both inner and outer raceways. The contact pressures are simulated under dynamic operating conditions, with radial force $F_r = 5\,kN$ and shaft angular speed $\omega = 477.5\,rpm$.

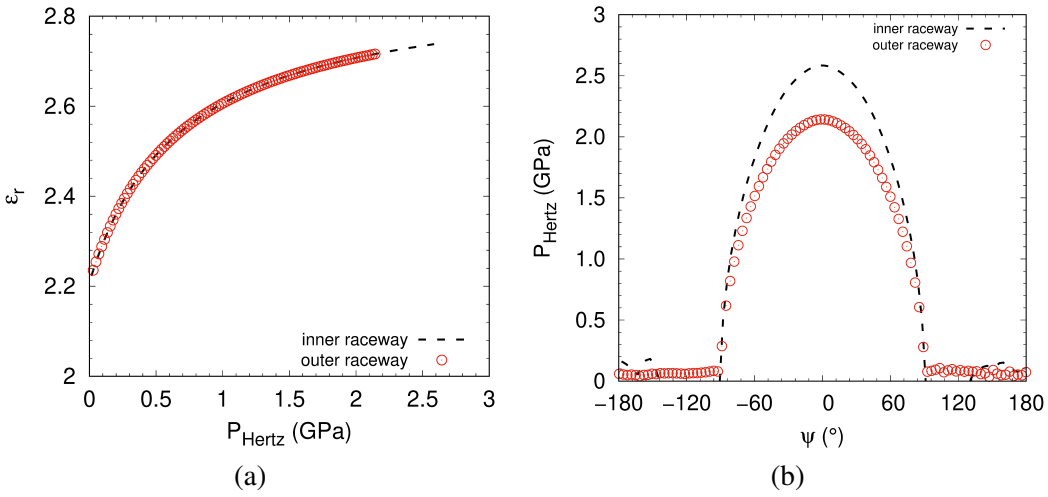

Figure 6: (a) Dielectric constant as function of Hertz contact pressure (ball bearing of 6208 series - PAO VG48 at 40° C) - (b) Hertz contact pressure as function of azimuth angle ψ

From electrical point of view, a single rolling element in contact with raceways can be considered as an equivalent circuit composed of capacitances between the inner and outer raceways contacts, which are in series. It should be pointed out that the cage components (PA66) are insulating which allows to consider the ball bearing as a set of capacitances in parallel (Fig. 7). The total capacitance of ball bearing is calculated by summing equivalent contact capacitances for all rolling elements located in the loaded zone.

$$C_{bearing} = \sum_{i=1}^{N_l} \left(\frac{C_{Hertz}^{inner,i} \times C_{Hertz}^{outer,i}}{C_{Hertz}^{inner,i} + C_{Hertz}^{outer,i}} \right) \tag{12}$$

with N_l the number of rolling elements in the loaded zone of ball bearing. The contact capacitances $C_{Hertz}^{inner,i}$ and $C_{Hertz}^{outer,i}$ between the i-th rolling element and inner-outer raceways, respectively, are determined according to the parallel-plate formula (8). It must be underlined that, unlike the case of experimental measurements, the capacitance model implemented in the digital twin does not take into consideration the contribution of capacitance between inner and outer ring and some background capacitance [20, 23].

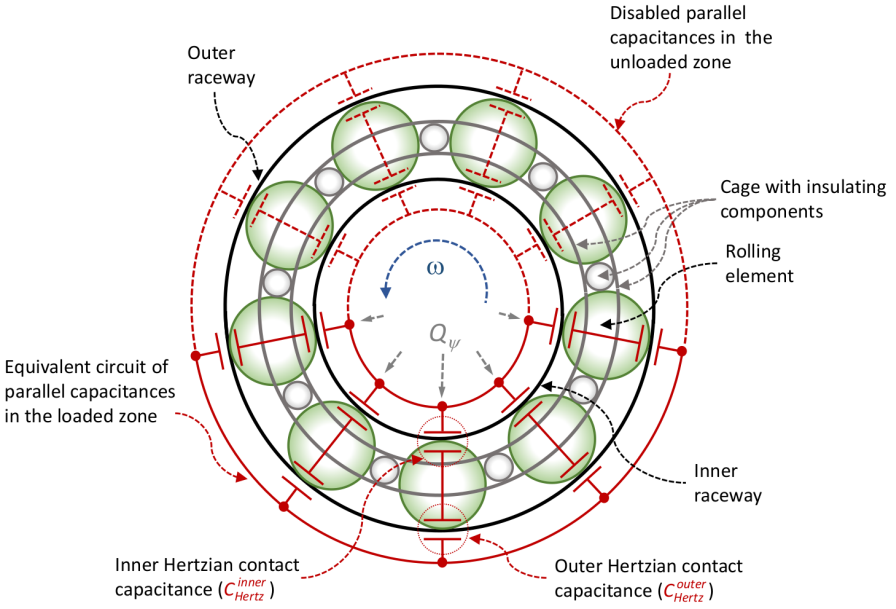

Figure 7: Flowchart of equivalent circuit with parallel capacitance of ball bearing

4 Numerical simulations and discussions

This section is dedicated to numerical simulations performed with the digital twin of ball bearing. The correlation between contact capacitance and fluid film thickness is investigated when ball bearing operates under imposed mechanical loading and fixed kinematic conditions. According to the parallel-plate capacitor formula the capacitance of the film fluid thickness is extracted considering a single rolling element after one revolution. Simulations are then carried out in order to exhibit the influence of the radial load F_r and diametral clearance P_d (Fig. 5-a) on the capacitance of the fluid film thickness. Comparisons with respect to experimental measurements [5] are performed in order to highlight the performances of the digital twin of ball bearing. Two kinds of lubricants are considered based on the experimental study given in [5], namely mineral oil and polyalphaolefin synthetic oil (PAO). In Table 2 are summarized the physical properties of both lubricants.

Lubricant	Mineral Oil	PAO VG48
Cinematic viscosity υ $\left(\frac{\eta}{\rho}\right)$ at 40° C $\left(mm^2/s\right)$	99.0	46.4
Pressure-viscosity coefficient ξ $\left(GPa^{-1}\right)$	24.5	16.5
Dielectric constant ε_r	2.3	2.1

Table 2: Properties of the lubricants

Figure 8-a depicts the sensitivity of the capacitance to the radial load F_r ranging over the interval $[1-7\ kN]$ in the case of mineral oil. The capacitance is proportional to F_r, which means that the higher the radial load F_r, the more the change of fluid film capacitance is. From a numerical point of view, when the rolling element loses the contact with rings of ball bearing the capacitances in series related to the inner and outer raceways are disabled (Fig. 7). In addition, as it can be observed in Figure 8-a, the predicted capacitance for $F_r = 5\ kN$ is in quite good agreement with the experimental measurements obtained with the same entrainment speed U_r in the case of 6306 ETN9 deep groove bearing

with a polymer cage [5].

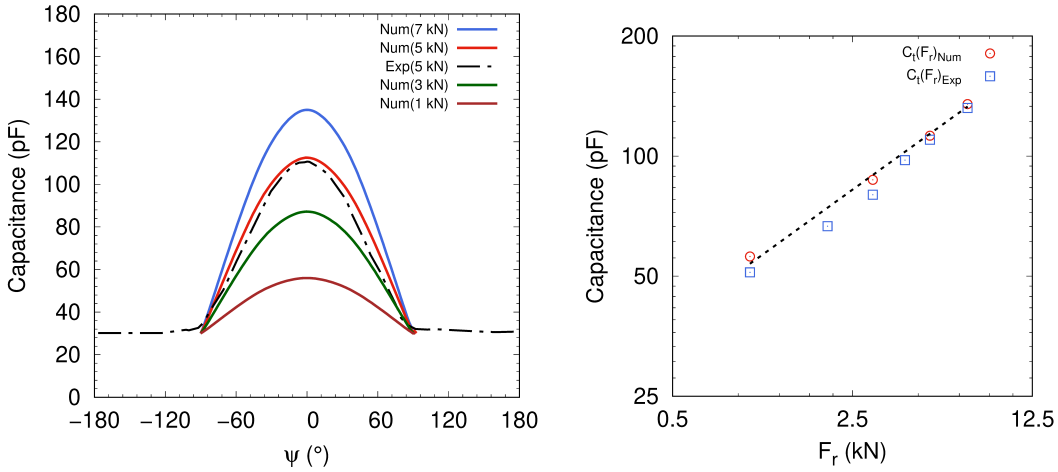

(a) (b)

Figure 8: (a) Capacitance distribution in the loaded zone with $P_d = 0$ and $U_r = 0.41\ m/s$ (ball bearing of 6208 series - Mineral Oil at $40°$ C) - (b) Capacitance at the maximum radial load position $(\psi = 0°)$ as function of F_r

For comparison purpose we have added to our numerical results the capacitance related to the background and the capacitance due to the space between inner and outer raceways. The equivalent capacitance due to these latter effects is about $30\ pF$ according to the experimental results given in [5]. Therefore, the additional capacitance is supposed to be of the same order of magnitude as for the simulated ball bearing of 6208 series (SKF 6208 TN9/DBGA). A good accordance with experimental measurements can also be observed on the curve fit applied to the numerical predictions for a zero azimuth angle ψ (Fig. 5-a) where the radial load reaches its maximum. This confirms that the digital twin of ball bearing is able to predict fluid film capacitance fairly close to experimental data.

The next simulation deals with the effect of the load parameter ε $\left(\varepsilon = \frac{1}{2} - \frac{P_d}{4 \times \delta_r}\right)$ on the capacitance distribution in the ball bearing by considering several values of $\frac{P_d}{D}$ ratio. The capacitance distribution in the loaded zone is plotted for three configurations, typically with negative clearance, zero clearance and positive clearance. The values of $\frac{P_d}{D}$ ratio that have been considered are summarized in Table 3.

$P_d\ (\mu m)$	-44.1	-25.2	0	25.2	44.1
$\frac{P_d}{D}$	-0.0035	-0.002	0	0.002	0.0035
ε	1.32	0.75	0.5	0.39	0.32

Table 3: The simulated clearances P_d and the corresponding load parameter ε

The effect of the diametral clearance P_d is well highlighted in Figure 9. Because of more contacts between elements and raceways in the case of $P_d < 0$, this increases the number of capacitances put in play of the electrical model (Fig. 7). As it can be observed in Figure 9, for $\frac{P_d}{D}$ ratio of -0.0035, corresponding to a load parameter ε of 1.32, the capacitances of the electrical model are all activated. Conversely, in the case of positive clearance more than $50\ \%$ of capacitances are disabled because of

reduced size of loaded zone (Fig. 9).

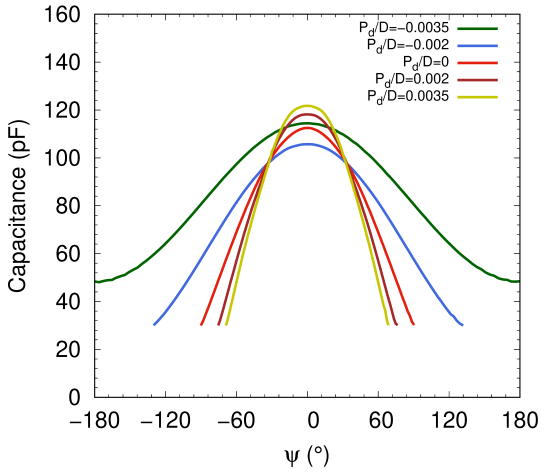

Figure 9: Capacitance distribution in the loaded zone with $F_r = 5000\ N$ and $U_r = 0.41\ m/s$

5 Conclusion

Through this work we have attempt to highlight the relevance of the digital twin when ball bearing operates under EHD lubrication regimes. A mechanical modeling based on a DEM has been carried out with the effort to provide realistic behavior of ball bearing in terms of kinematic parameters, contact stiffness and lubricant film effects. By means of a parallel-plate capacitor formula the capacitance of the fluid film thickness is numerically extracted with respect to the EHD lubrication regimes. Furthermore, qualitative and quantitative comparisons of the numerical predictions with experimental data pointed out the interest of the digital twin for industrial applications. Indeed, with the view to enhance the performance of industrial machines the digital twin could be a useful predictive tool for recommended lubrication regimes in bearings. However, the proposed modeling must be enhanced in order to take into account the effect of asperities in the EHD formulation.

References

[1] A.D. Roberts and D. Tabor. Fluid film lubrication of rubber—an interferometric study. *Wear*, 11(2):163 – 166, 1968.

[2] Wali M. Nozhat. Measurement of liquid-film thickness by laser interferometry. *Appl. Opt.*, 36(30):7864–7869, Oct 1997.

[3] Sébastien Murer, Fabien Bogard, Lanto Rasolofondraibe, Bernard Pottier, and Patrick Marconnet. Determination of loads transmitted by rolling elements in a roller bearing using capacitive probes: Finite element validation. *Mechanical Systems and Signal Processing*, 54-55, 02 2015.

[4] C. Machado, M. Guessasma, and V. Bourny. Electromechanical prediction of the regime of lubrication in ball bearings using Discrete Element Method. *Tribology International*, 127:69 – 83, 2018.

[5] K.A. Jablonka, R. Glovnea, and J. Bongaerts. Quantitative measurements of film thickness in a radially loaded deep-groove ball bearing. *Tribology International*, 119:239 – 249, 2018.

[6] C. Machado, M. Guessasma, and E. Bellenger. An improved 2D modeling of bearing based on DEM for predicting mechanical stresses in dynamic. *Mechanism and Machine Theory*, 113:53–66, 2017.

[7] M. Guessasma and C. Machado. Three-dimensional DEM modelling of ball bearing with lubrication regime prediction. *Lubricants*, 6(2), 2018.

[8] P.A. Cundall and O.D.L. Strack. A discrete numerical model for granular assemblies. *Geotechnique*, 29(1):47–65, 1979.

[9] B.J. Hamrock and W.J. Anderson. *Rolling-Element Bearings*. For sale by the National Technical Information Service, 1983.

[10] R.D. Mindlin and H. Deresiewicz. Elastic spheres in contact under varying oblique force. *ASME J. Appl. Mech.*, 20:327–344, 1953.

[11] K. H. Hunt and F. R. E. Crossley. Coefficient of restitution interpreted as damping in vibroimpact. *Journal of Applied Mechanics*, 42 (2):440–445, 1975.

[12] T. L. H Walford and B. J Stone. The sources of damping in rolling element bearings under oscillating conditions. *The Institution of Mechanical Engineers*, 197, 1983.

[13] A. Harnoy. *Bearing Design in Machinery: Engineering Tribology and Lubrication*. Mechanical Engineering. 2002.

[14] B.J. Hamrock and D. Dowson. *Ball Bearing Lubrication: Elastohydrodynamics of Elliptical Contacts*. John Wiley & Sons Inc, 1981.

[15] C. Mary, D. Philippon, N. Devaux, N. Fillot, D. Laurent, S. Bair, and P. Vergne. Bridging high pressure rheology and film-forming capacity of polymer-base oil solutions in ehl. *Tribology International*, 93:502 – 510, 2016. 41^{st} Leeds-Lyon Symposium on Tribology - Integrated Tribology.

[16] M. Masjedi and M. M. Khonsari. On the effect of surface roughness in point-contact EHL: Formulas for film thickness and asperity load. *Tribology International*, 82:228 – 244, 2015.

[17] T. E. Tallian. Paper 14: Rolling contact failure control through lubrication. *Proceedings of the Institution of Mechanical Engineers, Conference Proceedings*, 182(1):205–236, 1967.

[18] R. Stribeck. Ball bearings for various loads. *Trans. ASME*, 29:420–463, 1907.

[19] A. R. Wilson. The relative thickness of grease and oil films in rolling bearings. *Proceedings of the Institution of Mechanical Engineers*, 193(1):185–192, 1979.

[20] P. Brüser. *Untersuchungen uber die elastohydrodynamische schmierfilmdicke*. 1972.

[21] J.D. Jackson. *Classical Electrodynamics 2nd edition*. New York: Wiley, 1999.

[22] D. Dowson and G.R. Higginson. *Elastohydrodynamic Lubrication: the Fundamentals of Rollers and Gear Lubrication*. Oxford: Pergamon, 1966.

[23] K.A. Jablonka, R. Glovnea, and J. Bongaerts. Evaluation of ehd films by electrical capacitance. *Journal of Physics D: Applied Physics*, 45(38):385301–385309, September 2012.